A medium-energy ion scattering study of the Si(111)(√3×√3)R30°- Pb (β-phase) surface

2000 J. Phys.: Condens. Matter 12 4699

(http://iopscience.iop.org/0953-8984/12/22/303)

J. Phys.: Condens. Matter **12** (2000) 4699–4711. Printed in the UK PII: S0953-8984(00)10903-8

A medium-energy ion scattering study of the Si(111)($\sqrt{3} \times \sqrt{3}$)R30°– Pb (β-phase) surface

D J Spence†, S P Tear†§, P Bailey‡ and T C Q Noakes‡

†Department of Physics, University of York, Heslington, York Y010 5DD, UK
‡CLRC Daresbury Laboratory, Daresbury, Warrington WA4 4AD, UK

E-mail: spt1@york.ac.uk

Received 11 January 2000

Abstract. The Si(111)($\sqrt{3} \times \sqrt{3}$)R30°–Pb reconstruction has been studied using medium-energy ion scattering. The ion scattering data were taken from two different scattering geometries and compared with Monte Carlo simulations of the scattering curves, varying different structural parameters systematically until a suitable match between experiment and theory was obtained. A new structural model is proposed on the basis of these results.

1. Introduction

The growth of metals on semiconductors has been the focus for a large number of studies in ultra-high vacuums (UHV) and represents a substantial field in modern surface science. Research in this field is motivated from both a fundamental (crystal growth) and technological (Schottky barrier formation, fabrication of integrated circuits etc) interest. The Pb/Si(111) system provides a 'prototypical' metal–semiconductor surface due to the fact that Pb and Si have negligible mutual bulk solubility [1] leading to a non-reactive system with a relatively abrupt interface. In addition, for medium-energy ion scattering (MEIS), the large mass difference between Pb and Si allows the two peaks, corresponding to ions scattered from Pb and Si surface atoms, to be well resolved, even at quite low scattering angles.

Early LEED studies [2, 3] of this system revealed the presence of two ($\sqrt{3} \times \sqrt{3}$)R30° (hereafter $\sqrt{3}$) phases for Pb coverages of around 1 ML. For a Pb coverage of $\sim$ 1 ML, annealing to $\sim$ 300 °C gave rise to a $\sqrt{3}$ phase (designated the α phase) with a nominal coverage of 1.3 ML and heating further to $\sim$ 400 °C gave rise to another $\sqrt{3}$ phase (designated the β-phase) with a nominal coverage of 1/3 ML. In the case of the α-phase the $\sqrt{3}$ LEED pattern had the first order fractional beams missing, whereas this was not the case for the β-phase. It was suggested that the β-phase consisted of Pb adatoms in three fold hollow sites on an otherwise bulk-terminated Si(111) surface. For a Pb coverage of 1/6 ML, a further $\sqrt{3}$ phase has been observed, using STM [4, 5], and this is generally termed the γ-phase.

Doust and Tear [6] have performed the only quantitative structural study on the β-phase, using LEED I–V. There are two possible three fold co-ordinated sites on the surface, the T4 and the H3. The T4 site is located directly above a second-layer Si atom, whereas the H3 site is located directly above a fourth-layer Si atom. The LEED I–V study ruled out the H3 site, as no satisfactory agreement could be found between theory and experiment. The T4 site gave a

§ Author to whom any correspondence should be addressed.

0953-8984/00/224699+13$30.00

much better fit and a consequentially lower Pendry R-factor than for the H3 site. A later study by Roesler *et al* [7] using photoelectron holography agreed with this result. Doust and Tear's LEED I–V study also revealed substantial substrate shifts around the Pb adsorption site. The values for these shifts are shown in figure 1. It was stated, however, that although these values are close to the true solution, the search strategy had 'not fully converged on the solution'. The aim of the present study is, therefore, to refine this structural solution for the β-phase using the technique of MEIS. An extensive review of the technique of MEIS is available in the literature [8] as is a compilation of surface structures determined by ion scattering methods [9].

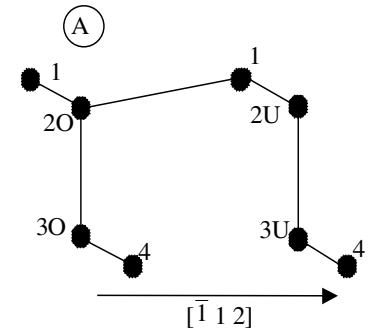

Separations	Bond length (Å) ± 0.05Å
A-1	2.55
A-2O	2.40
1-2O	2.32
1-2U	2.40
2O-3O	2.34
2U-3U	2.52
3O-4	2.30
3U-4	2.37

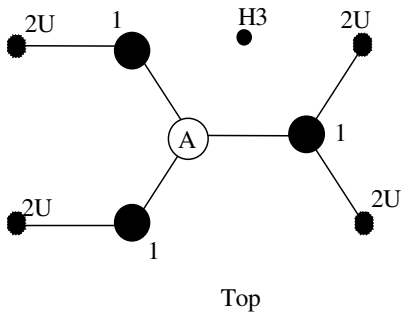

Figure 1. Schematic diagram, showing bond lengths, of the model determined by LEED [6].

2. Experiment

All MEIS experiments were performed at the MEIS facility at the CLRC Daresbury Laboratory, Warrington, Cheshire, UK. The facility has been described in detail elsewhere [10]. The Si(111) samples were lightly doped 100 Ω cm, n-type wafers and their temperature was monitored using an infra-red pyrometer. In order to obtain a clean substrate, the Si(111) was e-beam heated to $\sim$ 1200 °C for 1 minute. The temperature was monitored using an infra-red pyrometer. The sample was then slowly ($<$ 100 °C min^{-1}) cooled between 1000 °C and 600 °C to ensure an ordered surface. This process was repeated until a sharp 7 × 7 LEED pattern was obtained.

Approximately 0.5 ML of lead was deposited *in situ* from a Knudsen source at a rate of $\sim$ 0.3 ML min^{-1} with the substrate at room temperature. The β-phase was obtained by

heating the sample to $\sim$ 375 °C for 10–15 minutes in front of the LEED screen until a sharp $\sqrt{3}$ LEED pattern was obtained, with the excess Pb desorbing. Because of limitation in the optical pyrometer, the annealing temperature could not be measured accurately. Throughout sample preparation, the UHV chamber had a base pressure of less than $\sim 1 \times 10^{-9}$ mbar.

Ion scattering data were taken using 100 keV H^+ ions. The energy and angle of the scattered ions were detected by a two-dimensional position sensitive detector [12] incorporating microchannel plates, and analysed simultaneously by a toroidal electrostatic analyser [11]. Examples of data taken with this detector are given elsewhere [10, 13, 14]. Complete sets of data were collected at a total beam dose of 5 μC, corresponding to total beam dose of 6×10^{15} ions cm^{-2}, a figure roughly in line with other scattering experiments on semiconductors [9] and several times lower than the dose at which beam induced damage can be detected. The surface data was extracted by integrating the 2D data with respect energy over an angular range of 24°. The energy range of the integration was chosen to match the depth of the simulation and was varied to account for the change in ion path length with exit angle. The stopping power used was calculated using the TRIM program [15]. Two scattering geometries were used:

$[\bar{1}00]$ incidence/$[\bar{1}11]$ detection

normal incidence/$[\bar{1}11]$ detection.

These two geometries are illustrated in figure 2.

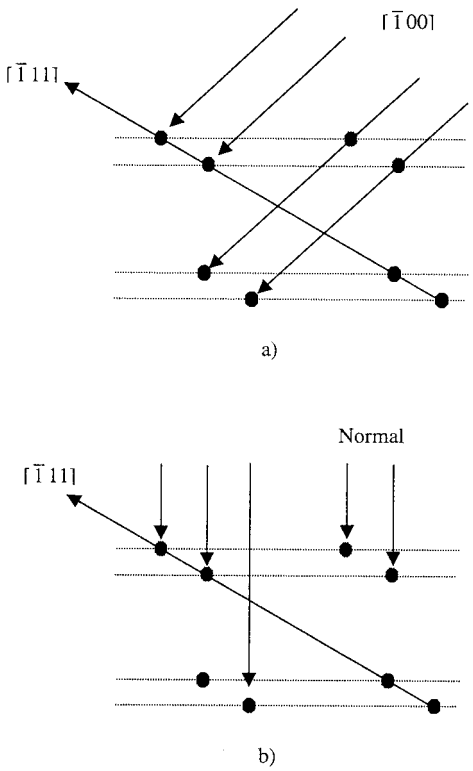

Figure 2. Schematic showing the two scattering geometries used in the MEIS experiments. (a) $[\bar{1}00]$ incidence /$[\bar{1}11]$ detection; and (b) normal incidence /$[\bar{1}11]$ detection.

In both cases, the ions are detected along the [$\bar{1}$11] direction. In this geometry, the second layer atoms are blocked by the first, making the blocking curves very sensitive to any changes in the spacing between the first two layers.

Due to the fact that the same detection geometry is used for both sets of data, at first glance it might appear that the blocking curves should be identical. However, the incident ion directions are quite different. The ⟨100⟩ incidence direction ensures that only the atoms in the ideally terminated top two layers of the crystal are illuminated, whereas the normal incidence geometry allows atoms in the fourth layer of the silicon to be illuminated. Furthermore, the presence of adatoms on T4 sites means that 1/3 ML of the second layer atoms should be shadowed and thus not 'see' the incoming ion beam in normal incidence.

All Monte Carlo simulations of the scattering curves were performed on a Sun Ultra 10 using the Vegas code [16, 17].

When comparing the simulations against experiment, a chi-squared R-factor was used, of the form:

$$R_\chi = \frac{1}{N}\sum_{n=1}^{N}\frac{\left(I_{\mathrm{exp}} - k \times I_{\mathrm{sim}}\right)^2}{I_{\mathrm{exp}}} \tag{1}$$

where I_{exp} and I_{sim} are the measured and simulated counts and N is the number of angular points. A number of different R-factors have previously been used in MEIS studies [9] and a detailed discussion on the choice of this particular R-factor and quantitative comparisons with alternatives has been given by Noakes *et al* [18].

When the R-value is calculated, the simulation is scaled so as to have the same average yield as the experimental data, with the angular variation in the Rutherford cross-section applied to the simulation in order to match correctly the experiment (the factor k in equation (1)). The simulation data are then compared directly with the experimental data. An R-factor (R_χ) value of unity then corresponds to a match limited only by statistical noise. The statistical basis of this particular R-factor means that the variation of R_χ around its minimum as a function of each structural parameter a provides an estimate of the precision of the structural parameter a_j according to [19].

$$\sigma_j^2 = 2/(\partial^2 R_\chi/\partial^2 a_j). \tag{2}$$

It should be noted that, unlike the R-factors used in the techniques of LEED [20] and PhD [21], R_χ scales with the number of counts (for the case of fit-limited data) and thus generally has no absolute meaning when compared between different experiments.

3. Results and discussion

3.1. Angular projection of the scattered ion yield from the Pb

Figure 3 shows the backscattering yield as a function of angle for ions scattered by Pb atoms in the [$\bar{1}$00]/[$\bar{1}$11] scattering geometry corrected for the angular variation of the Rutherford cross-section. No blocking features can be seen in the data, indicating that all of the Pb is located at the surface. Furthermore, if Pb islands had formed there would be some evidence, in the form of blocking features, due to scattering and blocking within the Pb islands. The complete lack of any such features strongly suggests that this is not the case. Importantly, the energy width of the Pb signal and the lack of a low energy 'tail' clearly shows that the Pb is located at the surface and not 'islanded' or migrated into the surface to form a bulk alloy.

The corresponding ion yield from the Pb in normal incidence is not shown because of its similarity to figure 3. Again, there is no sign of any blocking features in the data.

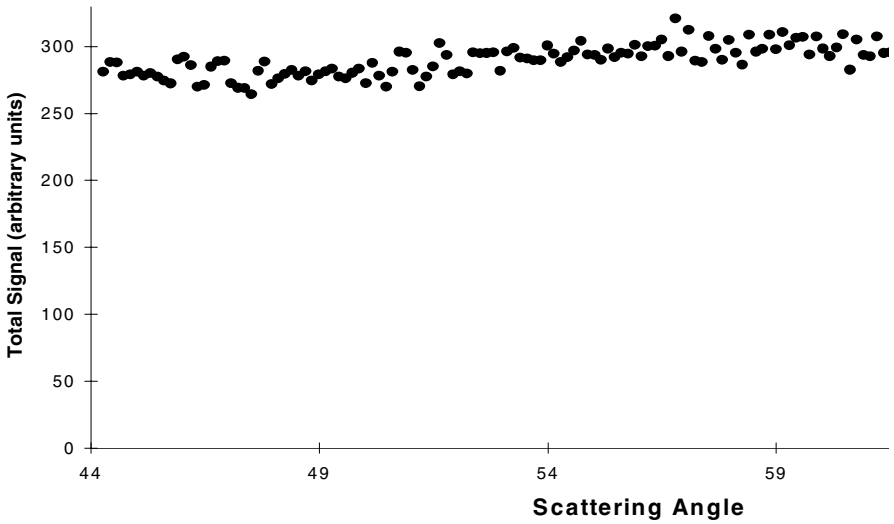

Figure 3. Angular projected ion scattering peak from the Pb for the [$\bar{1}$00]/[$\bar{1}\bar{1}$1] scattering geometry, corrected for the Rutherford cross-section.

3.2. Angular projection of the scattered ion yield from the Si

3.2.1. Sensitivity to the adsorption site. As a first test of the MEIS data, simulations were performed, for both geometries, for a bulk-terminated surface with Pb adatoms adsorbed onto either T4 or H3 sites. Although it has been established that the Pb adatoms reside on T4 sites [6, 7] it was felt that these simulations would provide useful information on the sensitivity of the MEIS scattering curves to changes in the surface structure.

Figure 4 shows the projected ion yield from the Si against angle compared with simulations for Pb adsorption onto either T4 or H3 sites. For comparative purposes, simulation of the bulk-terminated clean Si(111) surface is also shown. Although there is no absolute yield calibration, to allow some form of visual comparison to be made the yields of the experimental curves have been suitably scaled so as to have the average yield of the T4 and H3 simulations. The simulations are able to give an absolute yield in terms of number of layers contributing to the scattered ion yield and this unit has been used as the scale for the y-axis of the graphs.

As can be seen from figure 4, the simulations are broadly similar to the experimental data for adsorption onto either a T4 or a H3 site, differences in the simulated curves being extremely subtle. This highlights a difference between MEIS and LEED. LEED is a diffraction technique where interference of multiply scattered electrons leads to dramatic changes in the I–V curves for subtle changes in the surface structure. Due to this sensitivity, there is usually more than one minimum in R-factor space for a single structural search and it is sometimes difficult to determine whether the global minimum has been obtained rather than just a local one. For MEIS, the relative insensitivity of the blocking curves to slight changes in the structure means that its R-factor space is much smoother with a reduced risk of converging on a false minimum. However, due to the very subtle nature of the changes in the scattering curves arising from structural changes, any quantitative structural analysis of the Si(111)$\sqrt{3}$–Pb surface will require a detailed search in parameter space and high quality experimental scattering data. Furthermore, an examination of figure 4 reveals that the higher noise level of the normal incidence data (due to the lower number of counts in the higher scattering angle

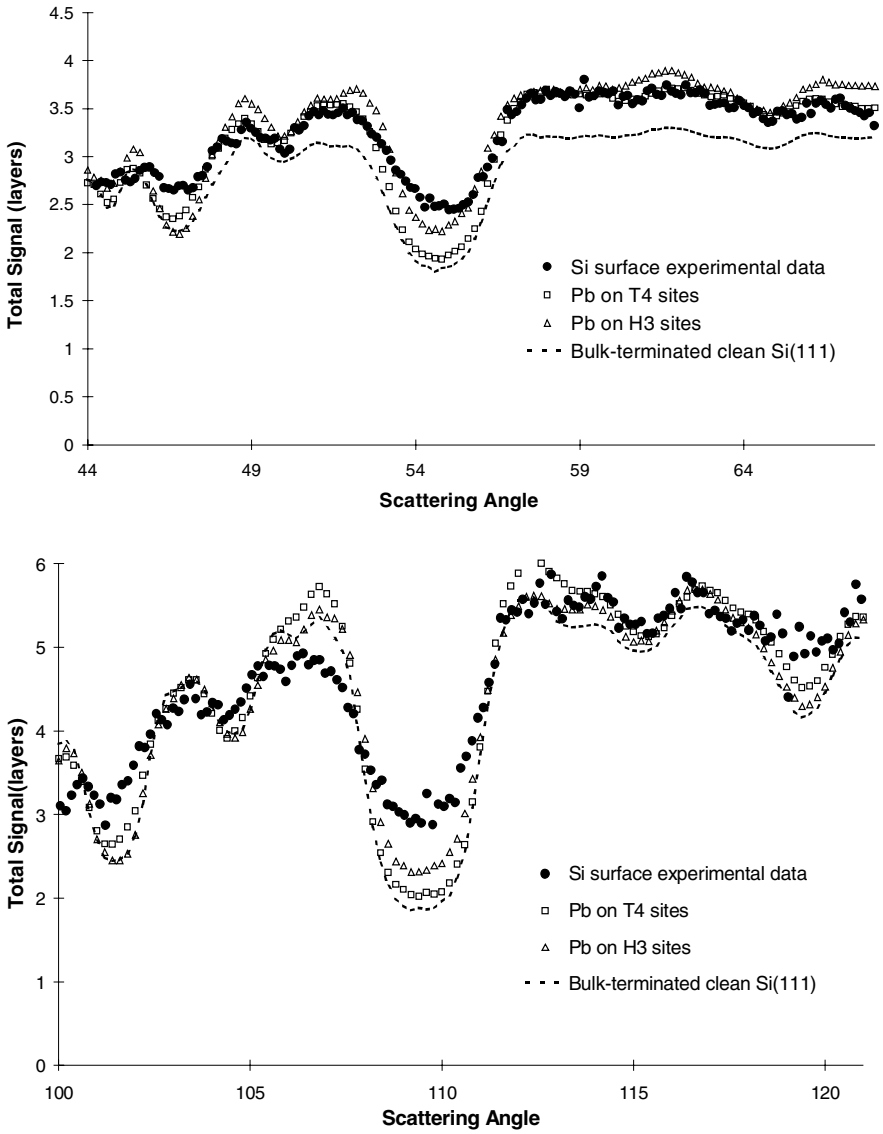

Figure 4. Comparison of experimental data with simulations for adatom adsorption on H3 and T4 sites. (a) $[\bar{1}00]/[\bar{1}11]$, (b) normal $/[\bar{1}11]$.

and correspondingly lower Rutherford scattering cross-section) is of a similar order to the differences in the illustrated simulations. This indicates that the $[\bar{1}00]/[\bar{1}11]$ data, with their far lower noise level, would be more appropriate as the basis for a detailed structural search in parameter space, at least in the initial stages.

3.2.2. Quantitative structural analysis. The relatively large (with respect to the bulk-terminated surface) unit-cell of the Si(111)$\sqrt{3}$–Pb surface means that, taking into account shifts down to the third layer, there are up to seven independent structural parameters which can be varied in the reconstruction. Layers four and beyond were not considered. These parameters are

shown in table 1 following the labelling scheme used in figure 1. All seven parameters can vary vertically but the first layer atoms may, in addition, shift laterally towards the adatom, making eight parameters in all. Parameter numbers of this magnitude are commonplace in LEED studies and there are established algorithms for performing automatic searches of parameter space. At present no such capability exists for MEIS (although developments are under way [22]) thereby limiting the number of parameters that can be varied simultaneously. Any structural search has, therefore, to be performed in stages, with some parameters varied before others.

Table 1. Structural parameters for the $\sqrt{3}(\beta)$ reconstruction, using the labelling scheme shown in figure 1. All atoms can shift vertically from their bulk positions. In addition, the first layer atoms can also shift laterally, towards the adatom.

Parameter	Description
A	Adatom height
1(V)	Vertical shift of first layer atoms
1(L)	Lateral shift of first layer atoms
2U	Vertical shift of second layer atoms below unoccupied T4 sites
2O	Vertical shift of second layer atoms below occupied T4 sites
3U	Vertical shift of third layer atoms below unoccupied T4 sites
3O	Vertical shift of third layer atoms below occupied T4 sites

The rms thermal vibrations used in the simulations were derived from the bulk Debye temperatures of Si and Pb [23]; 645 K for Si and 105 K for Pb, giving vibration amplitudes of 0.085 Å and 0.19 Å, respectively. For the adatom and top Si bi-layer, these vibrations were enhanced by a factor of $\sqrt{2}$ with respect to their bulk values. Simulations were performed for a series of different values for the vibration amplitude and it was found that small changes had a negligible effect on the positions of the blocking dips, the main effect being a change in the absolute yield. As the vibrational amplitude increases, the top layer atoms shadow sub-surface atoms less efficiently, leading to an increase in the absolute yield. In the case of this work, no absolute calibration could be made and so this effect is not significant.

The structural search began using Doust and Tear's LEED model [6]. Simulations were performed for this model and compared against experimental data for both scattering geometries. These comparisons are shown in figure 5 for both scattering geometries. In both cases, the data have been scaled so as to match the average yield of the simulation to enable a visual comparison to be made. For both geometries the match is visually quite good, although there is a markedly better agreement for the $[\bar{1}00]/[\bar{1}11]$ scattering geometry, shown in figure 5(a). The higher yield of the LEED model compared with the bulk simulation is very pronounced and is the result of shifts in the Si atomic positions at the surface. Surface relaxations tend to move atoms away from their bulk positions and hence cause shadowing of atoms deeper in the crystal to be less effective, leading to an increase in the detected absolute yield.

The next stage was to perform a series of simulations in which the structural parameters were varied systematically using the LEED model as the starting point. Due to the much higher number of counts of the $[\bar{1}00]/[\bar{1}11]$ data, the structural search used this dataset, and thus in the approach followed here, the normal $[\bar{1}11]$ data are used only as a verification of the model found using the $[\bar{1}00]/[\bar{1}11]$ data.

The four structural parameters, likely to be the most sensitive, that were initially varied are:

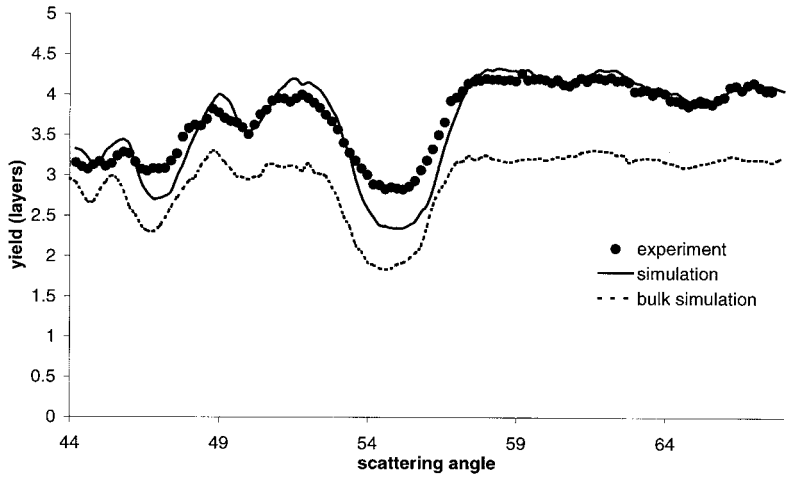

a)

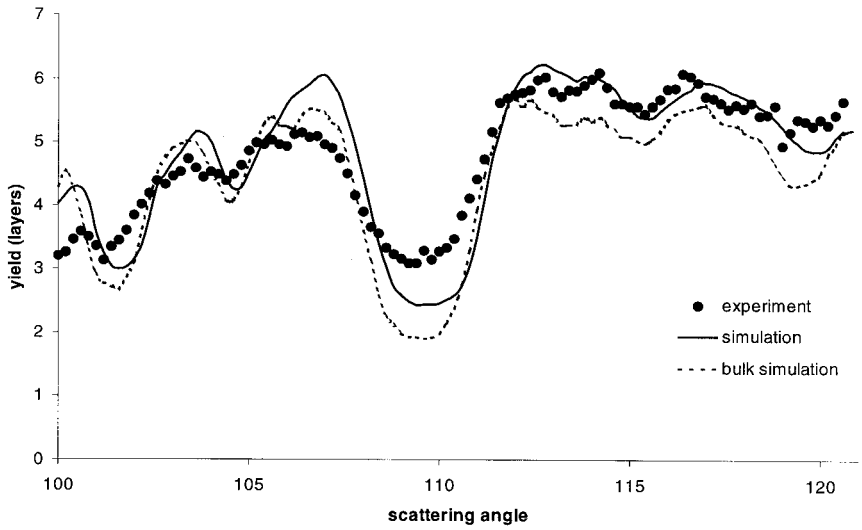

b)

Figure 5. Comparison of a simulation for the LEED model [6] against experimental data for (a) the [$\bar{1}$00]/[$\bar{1}$11] scattering geometry; and (b) the normal /[$\bar{1}$11] scattering geometry.

(i) The adatom height;
(ii) The first layer vertical shift;
(iii) The second/third layer atoms (occupied) vertical (constant bond length); and
(iv) The second/third layer atoms (unoccupied) vertical (constant bond length).

The three remaining parameters were fixed as follows. The lateral shift was fixed at its value determined from the LEED study. The second/third layer bond length was fixed and the displacements of the atoms below occupied and unoccupied T4 sites were taken as the average

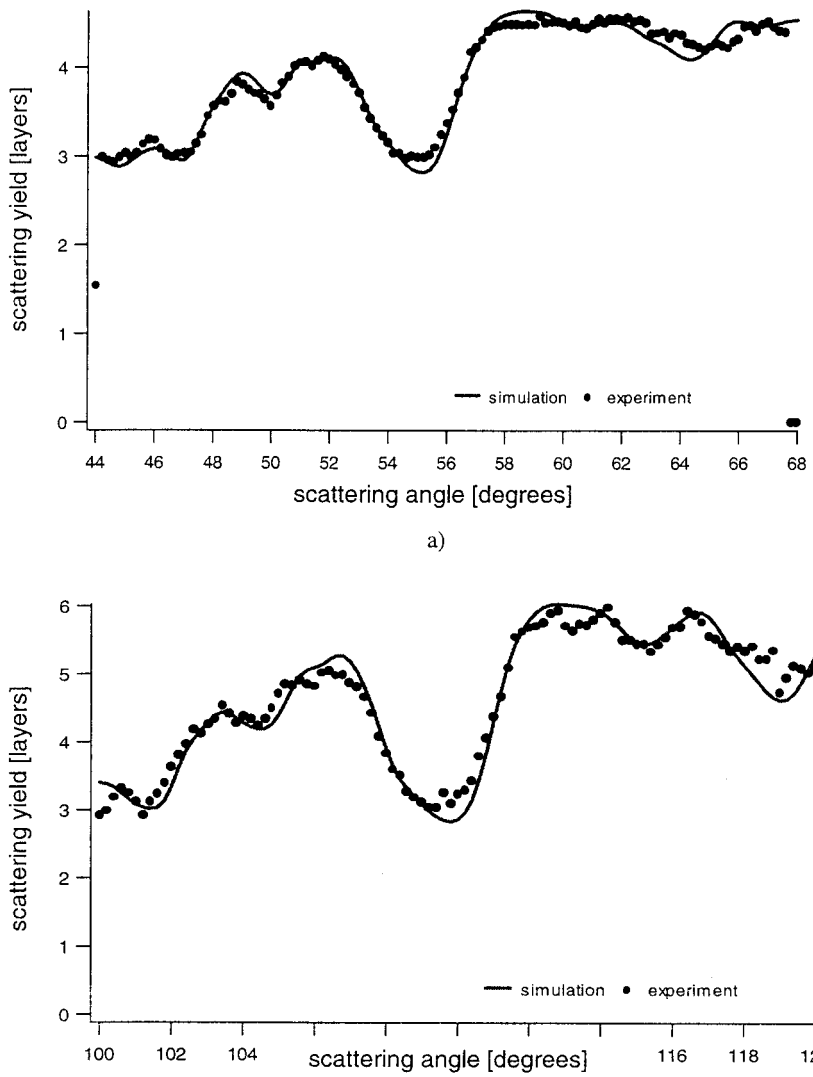

Figure 6. (a) Simulated scattering curve for the best structural solution, for the [$\bar{1}$00]/[$\bar{1}$11] geometry. (b) Normal incidence simulation for the model obtained from the [$\bar{1}$00]/[$\bar{1}$11] experimental data.

shifts of atoms in the second and third layers.

The non-fixed parameters were varied together in stages using 0.1 Å steps over a range of ±0.2 Å until they converged to a solution. The second/third layer atoms below occupied and unoccupied T4 sites were then varied independently, keeping the others fixed at the converged solution. In terms of the simulations, this is four parameters, using a step size of 0.1 Å with a ±0.2 Å range for each multiparameter simulation. After a new solution had been converged upon by varying these parameters, the positions of the adatoms and displacements of the

first layer (both vertical and lateral) were then varied again, using a ±0.2 Å range for each multiparameter simulation. Once a structural solution had been found for these parameters, a further refinement was undertaken in which they were varied by ±0.1 Å using 0.03 Å step sizes for the adatom height and the first layer (vertical) displacement. The lateral shift was also varied around its new value by ±0.1 Å, but with only a 0.05 Å step size. The final step was then to vary each of the parameters of the second and third layers by ±0.1 Å around their new values, with a 0.05 Å step size. The final shifts in the atomic positions obtained from this are shown in table 2 and the simulated scattering curve corresponding to these shifts, for the $[\bar{1}00]/[\bar{1}11]$ geometry, is shown in figure 6(a). A normal incidence simulation for this model, showing the agreement with the normal incidence data is shown in figure 6(*b*).

Table 2. Atomic shifts and errors, for the best model, obtained from the structural search using the $[\bar{1}00]/[\bar{1}11]$ data. Positive shifts towards bulk (vertical) and away from the adatom (lateral).

	Displacement from bulk positions (Å)	
Parameter	Initial model from LEED [6]	Model from MEIS
1st layer (vertical)	-0.08	-0.06 ± 0.02
2nd layer (lateral)	-0.11	-0.05 ± 0.03
2nd layer atoms (unoccupied)	-0.27	0.07 ± 0.02
2nd layer atoms (occupied)	0.11	0.44 ± 0.04
3rd layer atoms (unoccupied)	-0.11	0.12 ± 0.03
3rd layer atoms (occupied)	0.11	0.19 ± 0.04
Adatom height above first layer	1.43	2.14 ± 0.05

The simulations for the final structural model, shown in figure 6, match the experimental data somewhat better than the previous LEED model. This is most noticeable for the normal incidence geometry where the positions of the blocking dips are matched far more accurately than by the previous model. For $[\bar{1}00]$ incidence, figure 6(a), the lower scattering angle side of the experimental curve is matched closely by the simulation, significantly better than the earlier model.

Table 3. Bond lengths for the final structural solution, using the labelling scheme shown in figure 1.

Separations	Bond length (Å) ± 0.05 Å
A–1	3.04
A–2O	3.42
1–2O	2.52
1–2U	2.42
2O–3O	2.10
2U–3U	2.40
3O–4	2.29
3U–4	2.31

The bond lengths for this structural solution are shown in table 3.

A comparison between the structural solution, shown in table 3, and the LEED model, shown in figure 1, reveals that there are significant differences between the two structures. This is expected, considering that the LEED study had not fully converged on a solution. However, despite the differences, there are also some noticeable similarities between these two models. In particular, the shifts of the first layer, both vertically and laterally, are in approximate agreement. The shift in the atoms below occupied T4 sites are also in the same

Table 4. Bond lengths for the final structure, compared against bond lengths for other adatom-induced $\sqrt{3}$ reconstructions on Si(111) (bulk bond length= 2.35 Å). The bondlengths for the other structures are experimental results and the errors are not shown as the purpose of the table is purely to show trends in bond length expansions/contractions.

	Bond lengths (Å)					
Separations	Si(111)$\sqrt{3}$–Pb this work	Si(111)$\sqrt{3}$–Pb [6]	Si(111)$\sqrt{3}$–Sn [24]	Si(111)$\sqrt{3}$–Al [25]	Si(111)$\sqrt{3}$–Bi [26]	Si(111)$\sqrt{3}$–Ga [27]
A–1	3.04	2.55	2.55	2.49	2.39	2.50
A–2O	3.42	2.40	2.79	2.63	2.44	2.57
1–2O	2.52	2.32	2.33	2.41	2.55	2.43
1–2U	2.42	2.40	2.39	2.38	2.35	2.35
2O–3O	2.10	2.34	2.28	2.23	2.24	2.14
2U–3U	2.40	2.52	2.38	2.43	2.51	2.45

direction, although in the new model the shift is further towards the bulk. There is a difference in the position of the atoms below unoccupied T4 sites; the LEED model has the atoms move upwards by 0.27 Å, whereas this model has a very small shift downwards of 0.07 Å . The largest difference is in the position of the adatom. For the LEED model, this is 1.4 Å above the relaxed first layer atom, whereas from this work this value is 2.14 Å. In terms of their physical applicability, some measure can be gained from a consideration of the values of the distance of the adatom to the atom beneath the T4 site and the distance between the adatom and the first layer atoms. From the current study these values are 3.42 Å and 3.04 Å respectively, which compare with values of 2.40 Å and 2.55 Å respectively for the LEED study. In the case of the latter this places the adatom closer to the second layer atoms than it is to the first layer atoms to which it is bonded. For the MEIS model, although the bond length between the Pb adatom and first layer Si atoms is quite large, it is only a 4% expansion of the summation of the Pb and Si bulk atomic radii which are 1.74 Å and 1.18 Å respectively.

This structural solution is in good agreement with similar metal-adatom-induced $\sqrt{3}$ reconstructions on Si(111) [24–27] (table 4). In particular, the shortening of the bond length between the second and third layer atoms below occupied T4 sites (2O–3O) and the expansion of the bond length between the second and third layer atoms below unoccupied T4 sites (2U–3U) appear to be common features of adatom-induced $\sqrt{3}$ reconstructions. A further point of agreement is the expansion of the bond length between the first layer atoms and second layer atoms below unoccupied T4 sites (1–2U). This expansion is seen for all structures apart from the Si(111)$\sqrt{3}$–Bi [26] and Si(111)$\sqrt{3}$–Ga [27] surfaces where this bond length remains constant. In terms of the bond length between the first layer atoms and the second layer atoms below occupied T4 sites (1–2O), there does not appear to be a trend for either expansion or contraction of the bond length, with some systems exhibiting a contraction and others an expansion. The value derived in this study is, however, in good agreement with that derived for the Si(111)$\sqrt{3}$–Bi [26] surface.

The major discrepancy between the proposed structure and the other $\sqrt{3}$ structures is in the bond length between the Pb adatom and the first layer Si atoms. For the other structures this consists of a contraction of the summation of the metal and Si bulk atomic radii, whereas in this structure, there is an expansion. One possible reason for the discrepancy could be the relative insensitivity of the MEIS data to changes in the Pb adatom height. This is because Pb has a very low bulk Debye temperature and a correspondingly high bulk rms thermal vibration amplitude of 0.19 Å. This will also be enhanced at the surface (by a factor of $\sqrt{2}$ in the simulations) and lead to ineffective shadowing and blocking. In addition to this, the adatom coverage is only 1/3 ML, which will not produce a dominant contribution to the blocking curves. However, the position of the adatom must not be dismissed out of hand as the Pb–Si value for the bond length is still physically realistic.

4. Summary and conclusions

Using an initial model, previously proposed using LEED [6], a new model has been determined for the Si(111)$\sqrt{3}$–Pb (β-phase) reconstruction on the basis of a structural search using MEIS data acquired in the $[\bar{1}00]/[\bar{1}11]$ scattering geometry. When this structural model was simulated for the normal $[\bar{1}11]$ geometry, the scattering curve produced gave a good match with the experimental data. This new structure also shows many features in common with those previously proposed for equivalent structures on other metal-induced $\sqrt{3}$ surfaces.

References

[1] Olesinki R W and Abbaschian G J 1984 *Bull. Alloy Phase Diagrams* **5** 271
[2] Estrup P L and Morrison J 1964 *Surf. Sci.* **2** 465
[3] Saitoh M, Ouram K, Asano K, Shoh F and Hanawa T 1985 *Surf. Sci.* **154** 394
[4] Ganz E, Xiong F, Hwang I-S and Golovchenko J A 1991 *Phys. Rev.* B **43** 7316
[5] Gómez-Rodríguez J M, Veuillen J-Y and Cinti R C 1997 *Surf. Sci.* **377–379** 45
[6] Doust T N and Tear S P 1991 *Surf. Sci.* **251/252** 568
[7] Roesler J M, Sieger M T, Miller T and Chiang T-C 1995 *Surf. Sci.* **329** L588–92
[8] van der Veen J F 1985 *Surf. Sci. Rep.* **5** 199
[9] Watson P R 1990 *J. Phys. Chem. Data* **19-1** 85
[10] Bailey P, Noakes T C Q and Woodruff D P 1999 *Surf. Sci.* **426** 358
[11] Smeenk R G, Tromp R M, Kertsen H H, Boerboom A J H and Saris F W 1982 *Nucl. Instrum. Methods* **195** 581
[12] Tromp R M, Copel M, Reuter M C, von Hoegen M Horn, Speidell J and Koudijs R 1992 *Rev. Sci. Instrum.* **62** 2679
[13] Brown D, Noakes T C Q, Woodruff D P, Bailey P and le Goaziou Y 1999 *J. Phys.: Condens. Matter* **11** 1889
[14] Noakes T C Q, Bailey P, Hucknall P K, Donovan K and Howson M A 1998 *Phys. Rev.* B **58** 4934
[15] Ziegler J F *TRIM code* IBM Corporation, Yorktown Heights, NY, USA (http://www.research.ibm.com/ionbeams)
[16] Tromp R M and van der Veen J F 1983 *Surf. Sci.* **133** 159
[17] Frenken J W M, van der Veen J F and Tromp R M 1986 *Nucl. Instrum. Methods* B **17** 334
[18] Noakes T C Q, Bailey P and Woodruff D P 1998 *Nucl. Instrum. Methods* B **17** 1125
[19] Bevington P V 1969 *Data Reduction and Error Analysis for the Physical Sciences* (NewYork: McGraw-Hill)
[20] Pendry J B 1980 *J. Phys. C: Solid State Phys.* **13** 937
[21] Woodruff D P 1974 *Surf. Sci.* **43** 431
[22] Woodruff D P 1999 Private communication
[23] Kittel C 1976 *Introduction to Solid State Physics* 5th edn, (New York: John Wiley)
[24] Conway K M, MacDonald J E, Norris C, Vlieg E and van der Veen J F 1989 *Surf. Sci.* **215** 555
[25] Huang H, Tong S Y, Yang W S, Smith H D and Jona F 1990 *Phys. Rev.* B **42** 7483
[26] Wan K J, Guo T, Ford W K and Hermanson J C 1992 *Surf. Sci.* **261** 69
[27] Kawazu A and Sakama H 1988 *Phys. Rev.* B **37** 2704